

Advances in computer simulations of LPP sources for EUV Lithography

A. Hassanein and T. Sizyuk

Center for Materials under Extreme Environment, School of Nuclear Engineering
Purdue University, West Lafayette, IN, USA

ABSTRACT

Photon sources for extreme ultraviolet Lithography (EUVL) are still challenging problem to achieve high volume manufacture in the semiconductor industry. Currently EUVL community narrowed the research and developments to two directions: discharge produced plasma (DPP) assisted with trigger lasers and dual-pulse laser produced plasma (LPP) with mass-limited targets. Such complicated systems require extensive optimization to enhance the conversion efficiency (CE) and components lifetime and detail source optimization requires significant experimental and costly efforts.

We used our HEIGHTS simulation package to study and optimize LPP sources and to make realistic predictions as well as benchmarking of key experimental results. HEIGHTS package includes 3-D detail description of various integrated physical processes involved in LPP and DPP devices. The models are extensively tested and benchmarked separately in each physics phase of laser/target interaction as well as in the entire integrated system without any parameters adjustments or fittings.

We simulated LPP sources in full 3-D geometry using 10-50 μm tin droplet targets, as single droplets as well as distributed fragmented microdroplets with equivalent mass. We studied mass dependence, laser parameters efficiency, atomic and ionic debris generation, and optimization of EUV radiation output. Our modeling and simulation included all phases of laser target evolution: from laser/droplet interaction, energy deposition, target vaporization and fragmentation, ionization, plasma hydrodynamic expansion, thermal and radiation energy redistribution, and EUV photons collection as well as detail mapping of photons source location and size. We also predicted potential damage to the optical collection system from plasma energetic debris and the requirements for mitigating systems to reduce debris fluence. The debris effect on mirror collection system is analyzed using our 3-D ITMC-DYN Monte Carlo package. Modeling results were benchmarked against our CMUXE experimental studies for the in-band photons production and for debris and ions generation.

Keywords: EUV, LPP, HEIGHTS, CO₂ laser, mass-limited target, ITMC-DYN, debris mitigation

1. INTRODUCTION

Extreme ultraviolet (EUV) photons source is probably the main obstacle in the successful development of cost efficient system for manufacturing the next generation computer chips. The requirements for high EUV power, optical system and components lifetime, and efficient mechanisms for target delivery have narrowed investigators towards the development and optimization of dual-pulse laser sources with small liquid tin droplets.

The choice of optimum droplet size is related to the performance and cost efficiency of the entire LPP source. Reducing droplet size will reduce the fluences of energetic ions and atoms and fragments deposition on optical mirrors that will extend their lifetime. However due to several factors, such as the expansion of preheated and evaporated droplet to appropriate volume and density for optimum coupling with the main CO₂ laser [1] or due to desired hydrodynamic confinement effects during the main laser exposure, the droplet size for efficient EUV photons production should be at least 20 μm in diameter [2]. For further optimization, from the point of view of EUV power requirements for high volume production processes, increase of droplet size to 30 μm or larger is necessary [3]. This is also important for potential increase in main laser energy for higher throughput without loss of source efficiency, which is restricted for the 20 μm droplet [2].

We continued our modeling and analysis of LPP sources with small droplets using Nd:YAG for pre-pulse followed by CO₂ laser as the main pulse. Our previous simulations showed an increase of the conversion efficiency (CE) using pre-pulse, up to 1.3% for 10- μm droplet and up to 3% for 30 μm [3]. Smaller droplets, i.e., 10 μm and 20 μm were almost entirely vaporized; this means we used the full mass of these targets for mist (vapor-plasma) creation. Vapor

density was near uniformly distributed in the case of smaller droplets before the main CO₂ laser pulse at the optimum delay time between pulses. We predicted and used in our simulations the fourth harmonic of Nd:YAG laser for optimum droplet preheating and vaporization. We utilized the advantages of the 266 nm wavelength for pre-pulse stage that results in much higher vaporization rate with lower pulse intensity compared to 1064 nm laser, generated less energetic ions debris, and the complete vaporization of droplet resulted in less contamination of the optical mirrors from tin debris. In addition, as it will be shown in the comparative analysis of prepared vapor-plasma mist, the 266 nm wavelength can generate more confined plume preventing the escape of atoms and ions during plume evolution.

Current work presents simulation results for LPP sources with 50- μ m droplet, optimization of pre-pulse and main pulse lasers for efficient EUV output, details of droplet and fragments vaporization, and effect of mist composition on EUV photons output and MLM surface damage.

2. MIST CREATION FROM DROPLETS

Application of pre-pulsing for target preparation allowed significant increase in CE of LPP sources with small droplets. The highest CE for CO₂ lasers without pre-pulse, obtained in experiments with droplets up to 50 μ m, is $\sim 0.5\%$ [4]. Similar values were predicted using our HEIGHTS simulations [3]. Variation in parameters of CO₂ laser, i.e., increase of pulse intensity or spot size, do not significantly increase efficiency of such single pulse laser devices using small spherical targets. This is mainly due to high reflection of 10.6- μ m wavelength from solid/liquid tin, low critical density and therefore low evaporation of droplet by CO₂ laser, and low confinement of the developed plasma plume to efficiently absorb and reabsorb (after reflection) laser photons because of the hydrodynamic motion of plasma around droplet. The Nd:YAG laser gives higher CE from small droplets, up to 1.3%, however it is still much lower than the CE that can be obtained from planar targets.

Due to deeper penetration of Nd:YAG laser wavelength in vapor/plasma plume and therefore higher energy transmitted to the target, this laser is more suitable for the pre-pulse stage. And, for the same reason, the fourth harmonic of this laser can be more efficient in preparing the mist plume before the main pulse. We simulated the evolution of vapor/plasma mist from 50- μ m droplet utilizing various lasers.

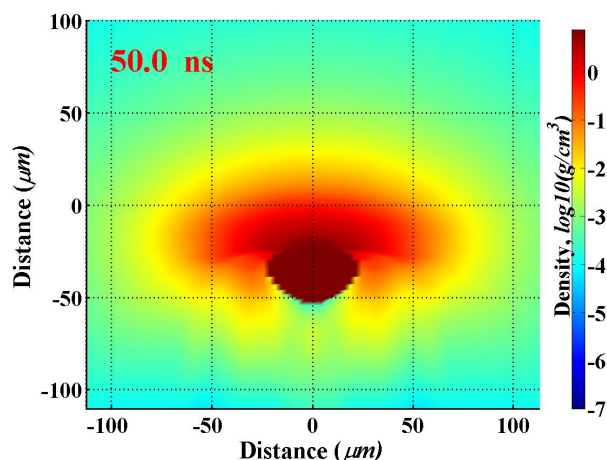


Figure 1. Mist density from 50- μ m droplet created by pre-pulse laser with 266 nm wavelength, 20 ns FWHM, 7.8 mJ, 50 μ m spot.

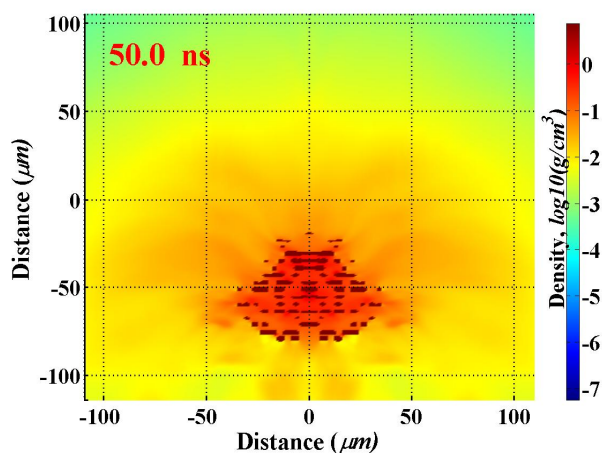


Figure 2. Mist density from 50- μ m droplet created by pre-pulse laser with 1064 nm wavelength, 10 ns FWHM, 400 mJ, 100 μ m spot.

Figures 1 and 2 show mass density distributions developed by pre-pulse lasers having 266 nm and 1064 nm wavelengths respectively. In the first case of 266 nm wavelength, laser with 7.8 mJ energy evaporated half of droplet. Laser with the longer wavelength evaporated approximately the same mass but at intensity 5×10^{11} W/cm², utilizing 400 mJ. For such high intensity laser we assumed droplet fragmentation during the laser pulse, therefore modeled droplet split into many fragments and distribution during 10 ns with velocity ~ 1 km/s predicted by recent experiments [5]. With the same evaporated mass, the last stated parameters of 1064 nm laser for the pre-pulse stage have several disadvantages.

First of all, laser energy required for the pre-pulse is comparable with energy of main pulse, and it will significantly decrease the conversion efficiency of entire system. Second, the maximum temperature of plasma plume developed by the long wavelength reached 120 eV, while shorter wavelength created plasma with temperature up to 14 eV. Hot plasma with high velocities, up to 150 km/s, includes ions with energies up to 12 keV. Energy of ions in plasma, created by 266 nm, did not exceed 700 eV for this system. Such plasma expanded more uniformly, which created better conditions for EUV emission during the main pulse.

Accurate description of energy transport in plasma by radiation fluxes is very important, especially for high intensities of laser pulse. Comprehensive 3-D model for radiation transport, verified and benchmarked, is critical for correct simulation of LPP devices. Two main separate modeling approaches for radiation transport (RT) calculations were developed, verified, and compared in the frame of our HEIGHTS package for various plasma science applications [6]. These include direct integration of radiation transport equations along photons path and Monte Carlo models with several novel weighting factors to enhance accuracy and reduce the extensive computational time. These approaches along with appropriate numerical techniques for multidimensional solution of laser LPP applications provide significant insight on the overall EUV production and collection.

We studied the effect of radiation transport on vaporization rate and modeled all phases of laser/droplet interaction, target vaporization, target hydrodynamic evolution, ionization, plasma expansion, thermal energy redistribution, and photon generation and transport. Figure 3 shows vaporization dynamics due to laser photons and to plasma with and without RT. After initial evaporation of sufficient mass layer for efficient laser absorption and the initiation of ionization processes, all laser photons are absorbed in the developed plasma/vapor plume. Photons generation in evolving plasma and their transport to target during and after laser pulse cause most target vaporization. The influence of plasma radiation on vaporization rate is even more pronounced for CO₂ laser even at low intensity, around 10¹⁰ W/cm², where more than 90% of evaporated mass was due to plasma radiation interaction with target (Fig. 4). The last example demonstrates effect of RT in full range on mist plume evolution from the distributed fragments, and as result on EUV photons source dynamics during main laser pulse.

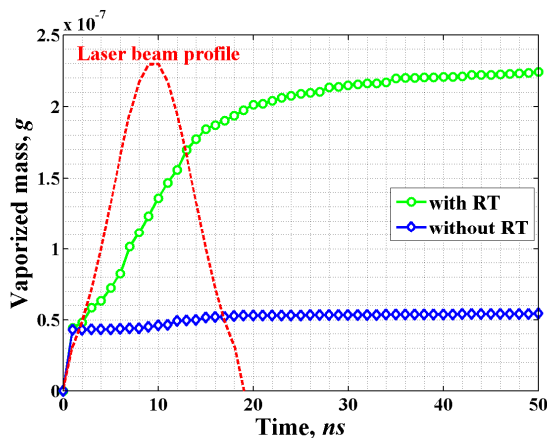


Figure 3. Vaporization of 50- μm droplet by laser photons and by LPP with 1064 nm wavelength laser, 10 ns FWHM, 400 mJ, 100 μm spot.

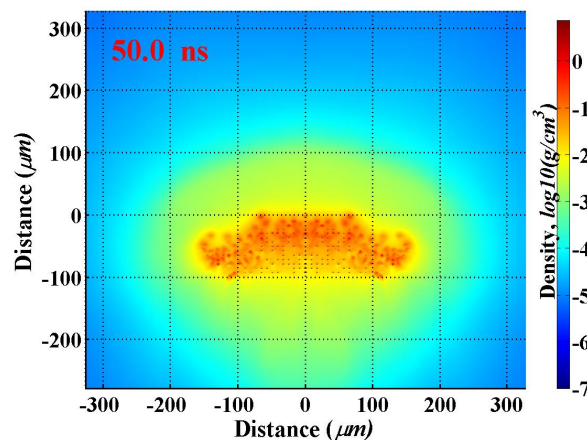


Figure 4. Mass density evolution of distributed fragments after CO₂ laser pulse heating with total mass equivalent to 50 μm droplet.

3. SOURCE OF EUV EMISSION AND CLEAN EUV POWER AT IF

We analyzed the dependence of CE on the delay time between pulses, on main laser energy, and on spot size for dual-pulse systems using 50- μm droplet as the target. Laser with 266 nm was used for initial mist creation from the droplet. Roughly half of droplet was vaporized by laser with intensity of 2×10^{10} W/cm² and 20 ns duration. We can neglect target fragmentation in this case and consider the target as single droplet during pre-pulse laser and subsequent time of plume expansion since such low pre-pulse laser intensity cannot cause significant droplet fragmentation [5]. Next, exploring various parameters of main laser we found that 500 ns is an optimum time for mist expansion for efficient coupling with the main CO₂ laser. Comparative analysis of mass density for optimized EUV output developed

from 50 μm , 20 μm , and 10 μm droplets showed that mist plume should have density of the order of or higher than 10^{-4} g/cm^3 to prevent laser energy loss due to laser photons transmission through matter (Figs 5-7). We obtained a maximum CE of around 1.3% in the case of 10 μm droplet and Fig.7 demonstrates that this value cannot be increased for such small target since the entire droplet was vaporized, mist was uniformly distributed, and plume matched the spot size of main laser that created the best possible conditions for EUV output from this droplet.

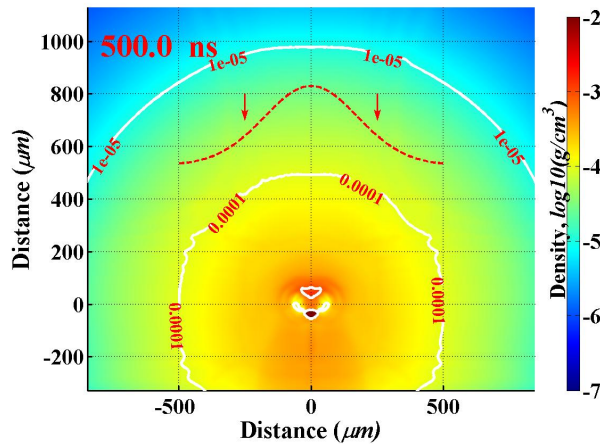


Figure 5. Mass density distribution developed by 266 nm laser from 50 μm droplet at optimum delay time for efficient coupling with CO_2 laser with 500 μm spot size.

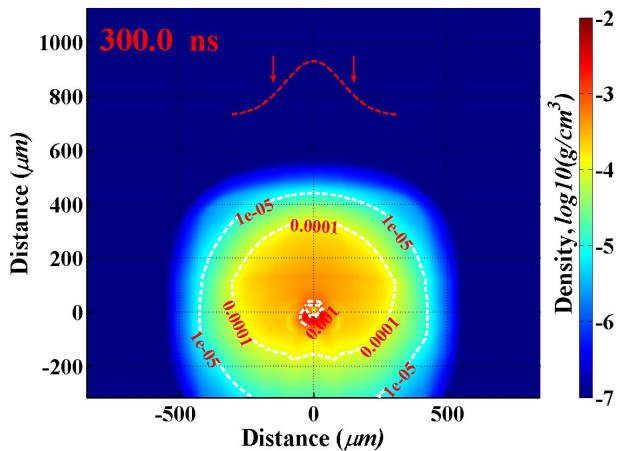


Figure 6. Mass density distribution developed by 266 nm laser from 20 μm droplet at optimum delay time for efficient coupling with CO_2 laser with 300 μm spot size.

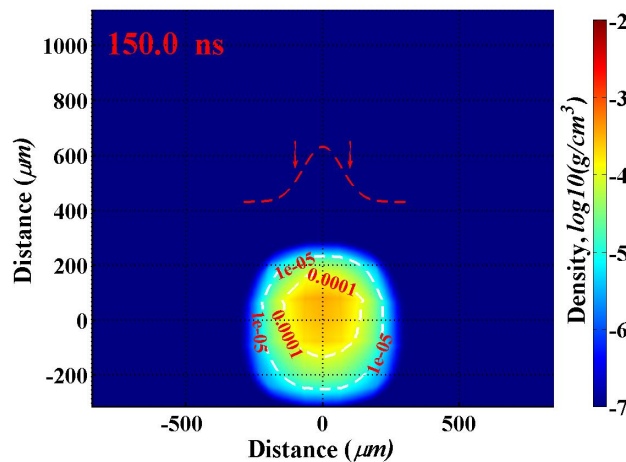


Figure 7. Mass density distribution developed by 266 nm laser from 10 μm droplet at optimum delay time for efficient coupling with CO_2 laser with 200 μm spot size.

To further analyze the above requirements for mist density, we simulated the heating of a large 50- μm droplet by CO_2 laser assuming droplet fragmentation during the pre-pulse stage and fragments distribution to surrounding volume within 300- μm diameter and studied the effect of the background density on CE. Fragments with size ~ 1 μm were randomly distributed in an ellipsoid volume with the assumed surrounding plume of vapor/plasma. The volume of surrounding plume was varied. We simulated the entire processes of laser interaction with fragments and vapor/plasma, taking into account laser photons and plasma photons absorption, reflections, and reabsorption after reflection in liquid/vapor/plasma phases. These results showed the same tendency in the requirements for background density, i.e., 10^{-4} g/cm^3 mass density occupied volume of around 10^{-3} cm^3 allows producing EUV source with 3.3% CE while 10^{-5} g/cm^3

produces 2.1% maximum CE, that is the same as from planar target. Matching of laser spot size to the area of fragments distribution in radial direction is very important in the last case.

We also investigated the potential use of larger droplet size and higher laser power to significantly increase the EUV output at the intermediate focus (IF). We calculated the EUV source size obtained from pre-plasma developed by 266 nm laser and distributed during 300 ns and 500 ns giving the optimum delay time for the considered 20- and 50- μm droplets and pre-pulse parameters. Figures 8 and 9 show EUV source size, location, and intensity (logarithmic values) collected in 5.5 sr during main laser pulse in plasma created from 50 μm and 20 μm droplets respectively.

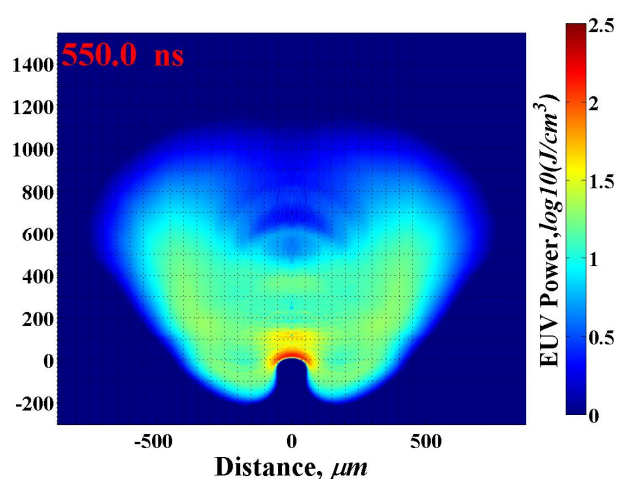


Figure 8. EUV source from 50- μm droplet preheated by 266 nm laser and distributed during 500 ns. Main laser: CO₂ with 500 μm spot and 350 mJ.

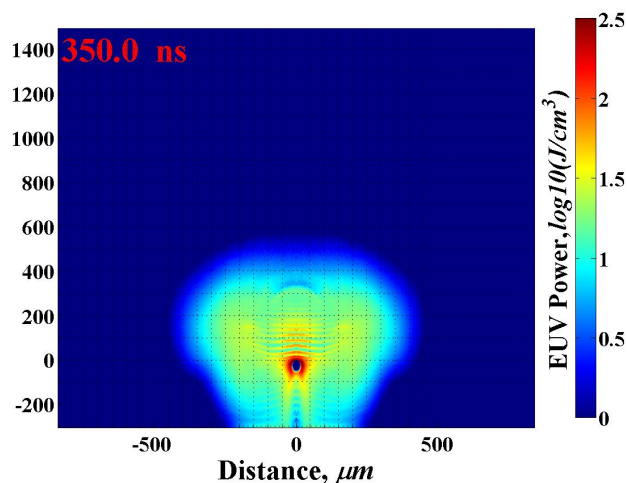


Figure 9. EUV source from 20- μm droplet preheated by 266 nm laser and distributed during 300 ns. Main laser: CO₂ with 300 μm spot and 140 mJ.

We obtained 11 mJ of EUV energy collected in 5.5 sr in LPP system using the larger droplet and 3.5 mJ with the smaller droplet. Taking into account Gigaphoton optical system parameters [7], EUV power of 600 W and 190 W respectively can be generated at IF for 100 kHz laser system.

Larger droplets allow obtaining higher CE and offer an opportunity for potential increase of source power. However larger source sizes may have difficulties in efficient EUV photons collection due to current requirements for etendue of the optical system [8]. Also, debris produced from the non-vaporized part of droplet can significantly decrease chamber components and optical system lifetime. Therefore, more detailed investigation of droplets with size starting from 25 μm is required to get efficient EUV source with minimum contamination and least damage to chamber components.

4. ENERGETIC IONS GENERATION AND MLM SURFACE DAMAGE

To accurately evaluate potential damage of multilayer mirror (MLM) surface by energetic tin ions, we calculated the energy spectra of ions in both single CO₂ laser and dual-pulse systems and compared our HEIGHTS results with our recent experiments at CMUXE. We found very good agreement between our modeling and our experimental data [9] as shown in Figs. 10 and 11. These results that can be used as additional benchmarking of the HEIGHTS package and predict initial debris parameters for the simulation of Sn ions interaction with mirror surface using our dynamic Monte Carlo code, ITMC-DYN, for ions/target interaction [10]. As it can be seen from Figs. 10 and 11, the single CO₂ laser pulse system produces much more energetic debris than the Nd:YAG due to the nature of energy deposition and the lower critical density for laser absorption. These unique results demonstrate the importance of detail inclusions of various processes in LPP devices during different phases of laser-target interactions.

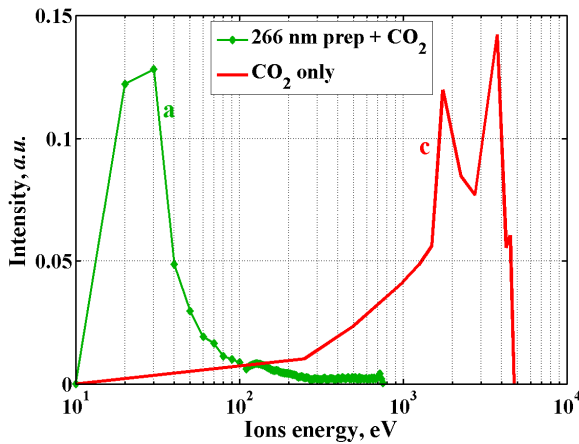


Figure 10. Ions kinetic energies of HEIGHTS modeling of planar Sn target; 15 mJ for pre-pulse and 90 mJ for CO₂ laser.

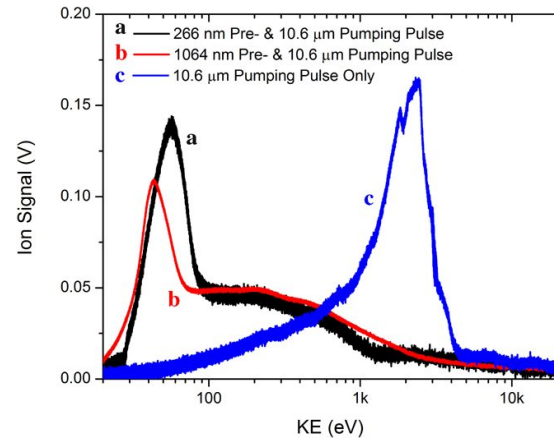


Figure 11. Ions kinetic energies in CMUXE experiments from planar Sn target; 15 mJ for pre-pulse and 90 mJ for CO₂ laser [9].

We then studied using our Monte Carlo dynamic model the interaction of Sn ion fluxes predicted from HEIGHTS and CMUXE with several layers of the MLM surface that consisted of 4.1 Si and 2.8 nm Mo alternating layers [11] with 3 nm Ru coating/capping layer at the surface [12].

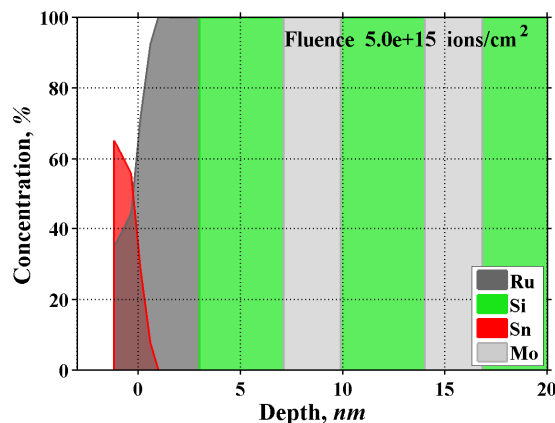


Figure 12. MLM surface response to Sn ions with Gaussian distribution of energies around 50 eV.

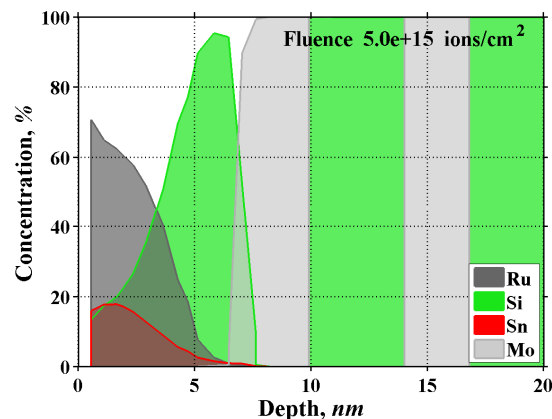


Figure 13. MLM surface response to Sn ions with Gaussian distribution of energies around 2.5 keV.

In the case of dual-pulse system, the pre-pulse laser with relatively low intensity did not produce high fluence of energetic ions. In the developed mist plume the main CO₂ laser photons interacted mainly with plasma surrounded by relatively dense region that prevented producing ions with high kinetic energies. The single pulse device using CO₂ laser in vacuum conditions of the LPP chamber produced plasma with much more energetic ions that can cause serious damage of mirror layers. The damage to MLM surfaces can include surface deposition or erosion as well as interatomic mixing of the first few MLM. While ions with low energy will interact mainly with the first coating layer, due to Sn deposition on the surface, buildup, and mixing with Ru capping layer as illustrated in Fig.12. However, ions with 1-3 keV energy can cause substantial erosion of Ru layer, tin implantation to deeper layers, and mirror interlayers mixing that can significantly degrade mirrors reflectivity as shown in Fig.13.

5. CONCLUSION

We studied and analyzed LPP sources using 10-50 μm tin droplet targets, as single droplets as well as distributed microdroplets with equivalent mass, to study mass dependence, laser parameters requirements, atomic and ionic debris generation, and to optimize EUV radiation output. Accurate computer simulation with sufficient details can be used with confidence to understand, design, and optimize LPP plasma devices and save significant time and cost compared to conducting numerous experiments. We extensively benchmarked HEIGHTS package and achieved good agreement with recent experimental results at CMUXE Lab and the dependence of ion debris energies on lasers parameters. Laser with shorter, 266 nm wavelength for pre-heating Sn droplets results in higher vaporization rate and lower temperatures of plasma plume. The higher vaporization rate allows near complete droplet vaporization and the lower temperatures of plasma plume reduce the fluence and energy of ions debris. Ions with low energy, in the order of 50 eV, will interact only with first coating layer by Sn deposition on the surface and mixing with Ru capping layer. Energetic ions with 1-3 keV energy can, however, cause significant erosion of Ru layer, tin implantations to deeper layers, and layers mixing at interface. This can cause significant degradation to mirrors reflectivity. Larger droplet, 50 μm for example, allows obtaining higher CE and offer reasonable pathway for potential increase in source power. However larger source sizes may cause difficulties in efficient EUV photons collection within the given etendue limits. Therefore, more detailed investigation of droplets with sizes starting from 25 μm is needed for designing efficient EUV source with minimum contamination and least damage to chamber components.

ACKNOWLEDGMENTS

This work is partially supported by the College of Engineering, Purdue University. We gratefully acknowledge the computing resources provided by the Fusion cluster operated by the Laboratory Computing Resource Center at Argonne National Laboratory.

References

- [1] Tomie, T., "Tin laser-produced plasma as the light source for extreme ultraviolet lithography high-volume manufacturing: history, ideal plasma, present status, and prospects", J. Micro/Nanolith. MEMS MOEMS 11(2), 021109 (Apr–Jun 2012).
- [2] Sizyuk, T. and Hassanein, A., "Optimization of extreme ultraviolet photons emission and collection in mass-limited laser produced plasmas for lithography application", J. Appl. Phys. 112, 033102 (2012).
- [3] Sizyuk, T. and Hassanein, A., "Enhancing extreme ultraviolet photons emission in laser produced plasmas for advanced lithography", Phys. Plasmas 19, 083102 (2012).
- [4] Fujimoto, J., Hori, T., Yanagida, T., Ohta, T., Kawasuji, Y., Shiraishi, Y., Abe, T., Kodama, T., Nakarai, H., Yamazaki, T., and Mizoguchi, H., "Development of laser-produced plasma based EUV light source technology for HVM EUV lithography" Proc. SPIE 8322, 83220F (2012).
- [5] Fujioka, S., Shimomura, M., Shimada, Y., Maeda, S., Sakaguchi, H., Nakai, Y., Aota, T., Nishimura, H., Ozaki, N., Sunahara, A., Nishihara, K., Miyanaga, N., Izawa, Y., and Mima, K., "Pure-tin microdroplets irradiated with double laser pulses for efficient and minimum-mass extreme-ultraviolet light source production", Appl. Phys. Lett. 92, 241502 (2008).
- [6] Sizyuk, V., Hassanein, A., Morozov, V., and Sizyuk, T., "Heights Integrated Model as Instrument for Simulation of Hydrodynamic, Radiation Transport, and Heat Conduction Phenomena of Laser-Produced Plasma in EUV Applications," ANL Report, ANL-MCS-CPH-06/56 (2006).
- [7] Mizoguchi, H., Abe, T., Watanabe, Y., Ishihara, T., Ohta, T., Hori, T., Yanagida, T., Nagano, H., Yabu, T., Nagai, S., Soumagne, G., Kurosu, A., Nowak, K.M., Suganuma, T., Moriya, M., Kakizaki, K., Sumitani, A., Kameda, H., Nakarai, H., Fujimoto, J., "100W 1st Generation Laser-Produced Plasma light source system for HVM EUV lithography", SPIE 7969 7969-08, 2011.
- [8] Bakshi, V., "EUV Source Technology: Challenges and Status", EUV Sources for Lithography, ed. V. Bakshi, SPIE Press, 2005, 7.
- [9] Freeman, J.R., Harilal, S.S., Hassanein, A., Rice, B., "Effect of prepulse laser wavelength on EUV emission from CO₂ reheated laser-produced Sn plasma", Applied Physics A (2012).
- [10] Sizyuk, T., and Hassanein, A., "Dynamic analysis and evolution of mixed materials bombarded with multiple ions beams", J. Nucl. Mater. 404, 60-67 (2010).

- [11] Bakshi, V., EUV Lithography, edited by V. Bakshi (ed.), SPIE Press, Bellingham, Washington, USA, Chapter 7, 333 (2009).
- [12] Bajt, S., et al., "Oxidation resistance and microstructure of ruthenium-capped extreme ultraviolet lithography multilayers", J. Microlith., Microfab., Microsyst. 5(2), 023004 (Apr–Jun 2006).